Comparison of Two Fourier Transform Methods in Modulation Measurement Profilometry

Min Zhong[1(✉)], Feng Chen[1], Chao Xiao[1], Peng Duan[1], Min Li[1], and Wenzao Li[2]

[1] College of Optoelectronic Engineering, Chengdu University of Information Technology, Chengdu 610225, China
zm1013@cuit.edu.cn

[2] College of Communication Engineering, Chengdu University of Information Technology, Chengdu 610225, China

Abstract. The modulation measurement profilometry encoding the spatial distribution information of specimen surface into the fringe defocus can realize the reconstruction of the specimen with complex surface shape. For this technique, the imaging axis of the CCD camera is coaxial with the projecting direction thanks to the application of a beam splitter mounting in the projection optical path. Without doing the phase unwrapping operation, it can accomplish shadow-free measurement for the specimen by extracting modulation values of the fringe pattern. The paper makes a comparison of the modulation retrieval in the conditions of fringe patterns with different surface profiles. Two Fourier transform methods are implemented in our computer simulation and practical experiment to show their performance in demodulating the modulation information from fringe patterns in optical 3D shape measurement.

Keywords: Surface measurements · Fourier transform · Image analysis · Modulation

1 Introduction

Three-dimensional surface shape measurement with the virtues of non-destructive, non-contact, high-resolution, high speed and ease of automation has become attractive to a profusion of industrial metrology, machine vision, robot simulation and automated manufacturing [1,2]. Among the existing optical three-dimensional shape measurement based on trigonometric measurement principle, Phase-shifting profilometry [3,4] is displayed more prominently thanks to its high measurement accuracy and low environmental vulnerability which is superior to that of other optical three-dimensional surface shape measurement technologies such as Four transform profilometry [5,6], Wavelet transform profilometry [7–9] and S-Transform profilometry [10–13]. However, as a multi-frame

X. Wu et al. (Eds.): QShine 2020, LNICST 381, pp. 192–208, 2021.
https://doi.org/10.1007/978-3-030-77569-8_14

fringes analysis technology, Phase shifting profilometry requires the projection of multiple patterns to reconstruct the shape surface of the specimen that speed may be sacrificed in favor of the resolution, and it's not competent for dynamic measurement. Therefore, the single-frame fringe analysis technology will be more widely utilized for measuring dynamically deformable shapes because only one single fringe projection is required to complete instantaneous deformation analysis. For this category of technique, the inherent problem of shadow and occlusion is inexorable because there is a certain angle between the projection and acquisition axes.

Some vertical measurement techniques [14–18] have been proposed in a bid to address this nontrivial problem, including modulation measurement profilometry and three-dimensional surface profilometry based on fringe contrast analysis, as distinct from the optical three-dimensional shape measurement based on the trigonometric measurement principle, applies a configuration with a feature that the projection axis coincides with the acquisition axis or the acquisition direction is the same as the projection direction. It not only avoids the effect of shadows and shutoff, but also solves the issue of phase truncating and spatial discontinuities. For this technology, the spatial distribution information of the specimen is encoded into the fringe defocus, so modulation values instead of phase information in the fringe pattern is required to be analyzed to accomplish the reconstruction.

There are two categories of the modulation measurement systems. For the first category, the grating moves in a direction parallel to the projected axis during the measurement process, and modulation values are extracted from the perspective of the entire two-dimensional fringe pattern. Phase-shifting method and two-dimensional Fourier transform method can be applied to realize the modulation calculation. For another category, a certain angle exists between the direction of the movement for the grating and that of the projection axis. Not only the above approaches, but also the one-dimensional Fourier transform method can be used to complete modulation retrieval. However, this method calculates the modulation information from an intensity curve formed by eponymous pixels from the series of the captured fringe patterns instead of each two-dimensional fringe pattern, and it is not applicable to the first type of system measurement. The one-dimensional Fourier transform method can be regarded as a kind of point-to-point operation instead of a global operation based on each entire fringe pattern analysis utilizing two-dimensional Fourier transform, which can retain more details of the specimen.

This paper gives a brief review of the theory for the modulation measurement in the second case (an angle exists), both one-dimensional Fourier transform method and two-dimensional Fourier transform method are used to extracting the fringe modulation distribution from two different viewpoints. Comparisons are made in both computer simulation and actual experiment to show their performance in demodulating the modulation information from fringe patterns in optical 3D shape measurement.

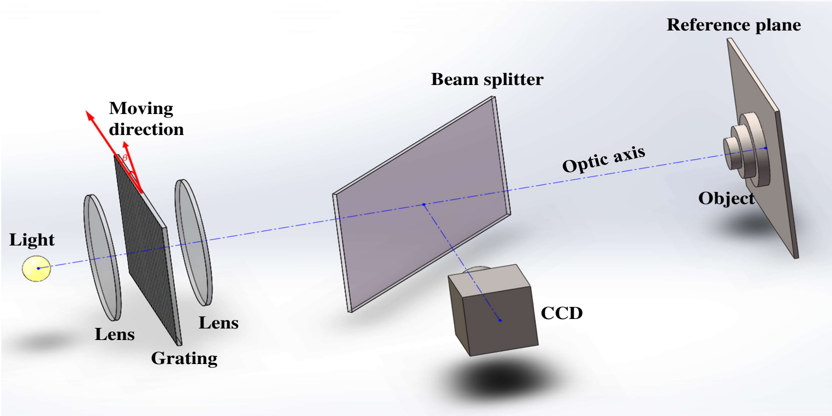

Fig. 1. The system configuration.

2 Principle

Figure 1 shows the system configuration of the modulation measurement profilometry. In this configuration, the grating is fixed on the translation platform and the normal of the grating plane is parallel to the optical axis. There is an angle (90°-β) existing between the bearings of the electric translation table and the projection optical axis. While the direction of detector is coaxial to the optic axis of projector. As such, this system offers a vertical measurement method against the problem of shadow and occlusion caused in triangulation system, which makes it possible to measure the specimen with complex surface. In the process of the measurement, the grating is driven by 1D precision translation platform, whose image will continually scan the specimen. Simultaneously, a CCD camera acquires the corresponding fringe patterns encoding the spatial

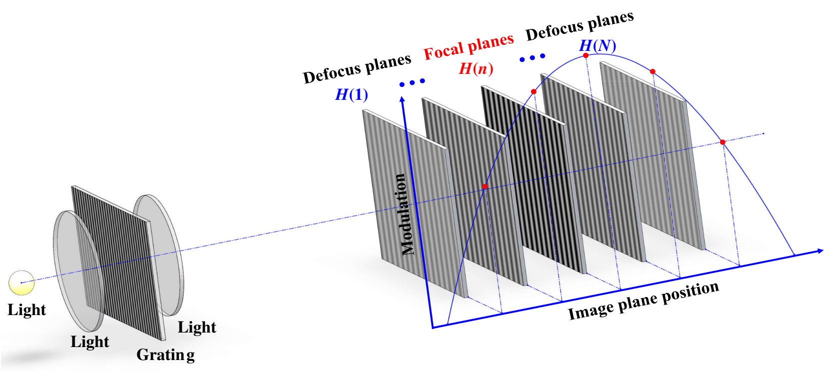

Fig. 2. Imaging principle.

distribution information of the specimen synchronously. Due to the existence of the angle (90°-β) between the direction of grating motion and the optical axis, a fixed phase shifting interval ($2\pi/N$, $N \geq 3$) appears for any two adjacent captured grating images. According to the imaging principle shown in Fig. 2, when project the image of the grating onto the specimen surface, the clearest fringe pattern with the largest modulation value observed by CCD camera will be produced on the focal plane. As the distance from the image plane to the focal plane increases, the image becomes more and more blurred. Therefore, a relationship between the modulation value and the image plane position can be formed as depicted in Fig. 2.

As shown in Fig. 1, in the actual measurement process, two sets of pulses with different time intervals will be sent by a controller. One set pulses are used to control the stepper motor to drive the grating to scan the specimen in succession, another set pulses are applied to trigger CCD camera to synchronously capture the grating image produced on the surface of the specimen that image acquisition will be synchronized with grating projection. Assuming that variable t represents the serial number of the collected image. Actually, variable t contains several other implicit meanings. When the CCD camera captures the t^{th} frame pattern, the t^{th} set pulses have been generated. Also, the grating derived by the 1D precision translation platform has been moved t times at an equal interval, the phase interval between the first grating image and the t^{th} grating image will be t times of $2\pi/N$ that the total phase shift is $t \cdot 2\pi/N$. The algorithm for the t^{th} frame fringe can be mathematically described as [16]

$$\begin{aligned} I_f(x,y,t) = {} & \frac{R(x,y)I_0(x,y)}{M^2} \\ & + \frac{R(x,y)C_0(x,y)}{M^2}\cos\left[2\pi f_0 x + \Phi_0(x,y) + \frac{2\pi(t-1)}{N}\right] \end{aligned} \tag{1}$$

$I_f(x,\ y,\ t)$ represents the light energy distribution of the t^{th} fringe. $R(x,\ y)$ is the reflectivity of the specimen. M is the transverse magnification. $I_0(x,\ y)$ and $C_0(x,\ y)$ respectively are the background intensity and projected fringe contrast. f_0 represents the grating frequency. $\Phi_0(x,\ y)$ is the initial phase. N represents the total phase shift numbers for one period. The value of t ranges from 1 to $T(t = 1,\ 2,\ 3,\ \ldots,\ T)$ that the grating moves T times throughout the whole scanning process.

$I_f(x,\ y,\ t)$ represents a clear image on the focal plane. While the image on the defocused plane with a distance γ from the focusing plane can be described as

$$I_d(x,y,t;\gamma) = h(x,y;\gamma) * I_f(x,y,t) \tag{2}$$

Where $I_d(x,\ y,\ t;\ \gamma)$ represents the blurred image. Symbol * is the convolution operation. The expression of $h(x,\ y;\ \gamma)$ is

$$h(x,y;\gamma) = \frac{1}{2\pi\sigma_h^2}e^{-\frac{x^2+y^2}{2\sigma_h^2}} \tag{3}$$

Where $\sigma_h = cr$. The value of c is a system parameter, and it often takes the value of [19].

Substitute Eq. 1 and Eq. 3 into Eq. 2, the out-of-focus image can be written to be

$$\begin{aligned} I_d(x, y, t; \gamma) = &\frac{R(x, y) I_0(x, y)}{M^2} + \frac{R(x, y) C_0(x, y)}{M^2} \\ &\bullet e^{-\frac{{f_0}^2 \sigma_h^2}{2}} \cos\left[2\pi f_0 x + \Phi_0(x, y) + \frac{2\pi(t-1)}{N}\right] \end{aligned} \tag{4}$$

The corresponding modulation distribution for the image with different degree of defocusing level can be defined as

$$\begin{aligned} M(x, y, t; \gamma) &= \frac{R(x, y)}{M^2} C_0(x, y) e^{-\frac{{f_0}^2 \sigma_h^2}{2}} \\ &= R(x, y) M_0(x, y) e^{-\frac{{f_0}^2 \sigma_h^2}{2}} \end{aligned} \tag{5}$$

Where $M_0(x, y)$ represents the modulation value on the focusing plane, which will be larger than that at any other defocusing plane.

3 Extraction of Modulation Values

3.1 Two-Dimensional Fourier Transform Method

When applying the two-dimensional Fourier transform method to calculate the modulation values, the result is obtained from the perspective of the entire two-dimensional image from the series of the captured fringe patterns. In mathematics, the convolution theorem states that under suitable conditions the Fourier transform of a convolution of two signals is the pointwise product of their Fourier transforms. Therefore, Eq. 2 can be written in the product form that

$$I_D(u, v, t; \gamma) = H(u, v; \gamma) \bullet I_F(u, v, t) \tag{6}$$

Where

$$\begin{aligned} H(u, v; \gamma) &= e^{-\frac{u^2+v^2}{2\sigma_h^2}} \\ I_F(u, v, t) &= \frac{R(u, v) I_0(u, v)}{M^2} \delta(u, v) \\ &+ \frac{R(u, v) C(u, v)}{2M^2} \delta(u - f_0, 0) e^{i\{\Phi_0(u,v) + \frac{2\pi(t-1)}{N}\}} \\ &+ \frac{R(u, v) C(u, v)}{2M^2} \delta(u + f_0, 0) e^{-i\{\Phi_0(u,v) + \frac{2\pi(t-1)}{N}\}} \end{aligned} \tag{7}$$

According to Eq. 6 and Eq. 7, the out-of-focus image in the frequency domain can be expressed as

$$I_D(u, v, t; \gamma) = I_{D(0)}(u, v, t; \gamma) + I_{D(1)}(u, v, t; \gamma) + I_{D(-1)}(u, v, t; \gamma) \tag{8}$$

Where

$$
\begin{aligned}
I_{D(0)}(u,v,t;\gamma) &= \frac{R(u,v)I_0(u,v)}{M^2}\delta(u,v) \\
I_{D(1)}(u,v,t;\gamma) &= \frac{R(u,v)C(u,v)}{2M^2}\delta(u-f_0,0)e^{i\{\Phi_0(u,v)+\frac{2\pi(t-1)}{N}\}}e^{-\frac{{f_0}^2\sigma_h^2}{2}} \\
I_{D(-1)}(u,v,t;\gamma) &= \frac{R(u,v)C(u,v)}{2M^2}\delta(u+f_0,0)e^{-i\{\Phi_0(u,v)+\frac{2\pi(t-1)}{N}\}}e^{-\frac{{f_0}^2\sigma_h^2}{2}}
\end{aligned}
\tag{9}
$$

Where $I_{D(0)}(u, v, t; \gamma)$ and $I_{D(1)}(u, v, t; \gamma)$ respectively represent the zero and the fundamental frequency component. $I_{D(-1)}(u, v, t; \gamma)$ is the conjugate of the $I_{D(1)}(u, v, t; \gamma)$. Select an appropriate filter window to extract the fundamental frequency part and then apply the inverse Fourier transform. The modulation value can be obtained by taking the absolute value of the obtained result.

$$
\begin{aligned}
M_{2DFFT}(x,y,t;\gamma) &= \left|\frac{R(x,y)}{2M^2}C_0(x,y)e^{i\{\Phi_0(x,y)+2\pi(t-1)/N\}}e^{-\frac{{f_0}^2\sigma_h^2}{2}}\right| \\
&= \frac{R(x,y)}{2M^2}C_0(x,y)e^{-\frac{{f_0}^2\sigma_h^2}{2}} \\
&= \frac{1}{2}R(x,y)M_0(x,y)e^{-\frac{{f_0}^2\sigma_h^2}{2}}
\end{aligned}
\tag{10}
$$

When making a comparison between Eq. 10 and Eq. 5, it becomes apparent that there is only one difference (constant 1/2), which means that the modulation distribution of out-of-focus image can be acquired by multiplying constant 2.

Two-dimensional Fourier transform method is a global analysis method. The modulation value of any pixel in the fringe pattern is extracted by taking advantage of the information of pixels in the entire two-dimensional fringe pattern. Therefore, even if a pixel in the fringe has no data, a modulation value for this pixel can be estimated based on the information of surrounding pixels, which implies that the sensitivity of this method is not high enough in detection of minor defects. Besides, the application of the filtering operation makes this approach fail to retain the details of the specimen, which will smooth the steep edges and corners, bring down a steep slope.

3.2 One-Dimensional Fourier Transform Method

When utilizing the one-dimensional Fourier transform method to realize the modulation acquisition, the calculation result is completed from an angle of an intensity curve formed by eponymous pixels from the captured images. Therefore, it is a kind of point-to-point operation instead of a global operation based on each entire fringe pattern analysis.

As shown in Fig. 3, points at the same position (x, y) are extracted from this series of images, and finally the curve $I(t)(x, y)$ (the blue curve, the red one represents its outline) shown in the right figure can be formed. Based on Eq. 1, curve $I(t)(x, y)$ from the definite point (x, y) of the fringes can be simply expressed as

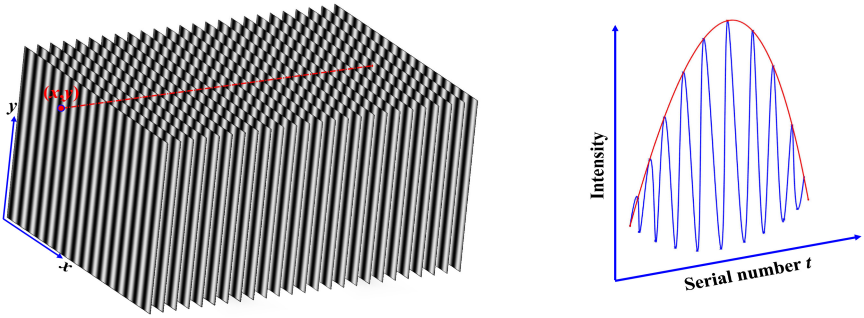

Fig. 3. The curve $I(t)(x,\ y)$. (Color figure online)

$$I_d(t)|_{(x,y)} = \frac{R}{M^2}\left\{I_0 + C_0 e^{-\frac{{f_0}^2\sigma_h^2}{2}} \cos\left[\varPhi + \frac{2\pi(t-1)}{N}\right]\right\}\Big|_{(x,y)} \tag{11}$$

For the same position $(x,\ y)$ on the fringe patterns,$\varPhi = 2\pi f_0 x + \varPhi_0$ is a constant. Do Fourier transform operation on Eq. 11 that

$$I_{D'}(t)|_{(u,v)} = I_{D'(0)}(t)\Big|_{(u,v)} + I_{D'(1)}(t)\Big|_{(u,v)} + I_{D'(-1)}(t)\Big|_{(u,v)} \tag{12}$$

Where

$$\begin{aligned} I_{D'(0)}(t)\Big|_{(u,v)} &= \frac{RI_0}{M^2}\delta(u,v) \\ I_{D'(1)}(t)\Big|_{(u,v)} &= \frac{RC}{2M^2}\delta(u-f_0,0)e^{i\{\varPhi+\frac{2\pi(t-1)}{N}\}}e^{-\frac{{f_0}^2\sigma_h^2}{2}} \\ I_{D'(-1)}(t)\Big|_{(u,v)} &= \frac{RC}{2M^2}\delta(u+f_0,0)e^{-i\{\varPhi+\frac{2\pi(t-1)}{N}\}}e^{-\frac{{f_0}^2\sigma_h^2}{2}} \end{aligned} \tag{13}$$

$I_{D'(0)}(t)\Big|_{(u,v)}$ denotes the zero-spectrum component of the curve, $I_{D'(1)}(t)\Big|_{(u,v)}$ and $I_{D'(-1)}(t)\Big|_{(u,v)}$ respectively represent the fundamental spectrum component of the curve. The utilization of a proper filter can make the acquisition of useful fundamental component come true, and then doing inverse Fourier transform. Modulation value for each fringe at position $(x,\ y)$ can be finally obtained by taking the absolute value of the result.

$$\begin{aligned} M_{1DFFT}(t)|_{(x,y)} &= \left|\frac{R}{2M^2}C_0 e^{i\{\varPhi+\frac{2\pi(t-1)}{N}\}}e^{-\frac{{f_0}^2\sigma_h^2}{2}}\Big|_{(x,y)}\right| \\ &= \frac{R}{2M^2}C_0 e^{-\frac{{f_0}^2\sigma_h^2}{2}}\Big|_{(x,y)} \\ &= \frac{1}{2}RM_0 e^{-\frac{{f_0}^2\sigma_h^2}{2}}\Big|_{(x,y)} \end{aligned} \tag{14}$$

Comparing Eq. 14 with Eq. 5, modulation distribution of out-of-focus image for point (x, y) can be calculated by multiplying constant 2. While the modulation maps of the whole images can be obtained by repeatedly doing the above operation for every point in the fringe patterns. For this method in modulation retrieval, the calculation result for each pixel in a fringe pattern in effect terminates the influence from the information of its neighbor pixels. That is, the operation of each pixel in the entire fringe pattern is independent of each other. The frequency spectrum of a curve by one-dimensional Fourier transform method is simpler than that of an image by two-dimensional Fourier transform method. Moreover, the generation of high-frequency components can be effectively avoided by appropriately selecting the scanning range, which refrains from spectrum aliasing between fundamental frequency and high order frequency. Obviously, due to the simple spectrum, it is easy to extract useful fundamental frequency information to retain more details of the specimen.

4 Simulation

In the actual application, the surface of the tested object is unpredictable. This section will make a comparison of the performance of the two Fourier transform methods in the reconstruction of two different surface profiles.

The main parameters are set as following. Both the background intensity and the fringe contrast are 0.5 $(I_0(x, y) = 0.5, C_0(x, y)) = 0.5$. The reflectivity factor is set to be $R(x, y) = 0$, The frequency of the grating is $f_0 = 1/6$ pixel^{-1}, the focal length and the diameter of the lens respectively are $f = 58$ mm and $d = 40$. In the scanning process, a total of 160 frames of fringes were collected by CCD that $T = 160$. The size of each image is 264×264 pixels. To match reality more exactly, random noise of 3% fringe intensity is added in each image. All the simulations are performed on MATLAB platform.

4.1 Comparison of Smooth Surface

The first tested object we used is the PEAKS function. It has an absolute height of 60 mm as shown in Fig. 4(a). Figure 4 (b) shows the 60th frame of captured images. Both one-dimensional Fourier transform method (1DFT) and Two-dimensional Fourier Transform method (2DFT) are used to calculating the modulation values of the images, and the performance for the 60th frame of captured images obtained by the two methods are respectively shown in Figs. 4 (c) and (d). It is palpable that there are many small spots in Fig. 4 (c), while the edges in Fig. 4 (d) are blurred. The reconstruction result and error distribution for the two approaches are respectively shown in Figs. 5 (a)–(d). The standard deviation errors (mean square error RMS) are 0.353 mm by 1DFT and 0.144 mm by 2DFT. Obviously, for the tested object with smooth surfaces, there are many burrs on the surface shape obtained by 1DFT. While for 2DFT, it softens the steep area even though the smoothness of the surface is preserved. In order to illustrate features clearly, Figs. 6(a)–(c) show a small area (rows:

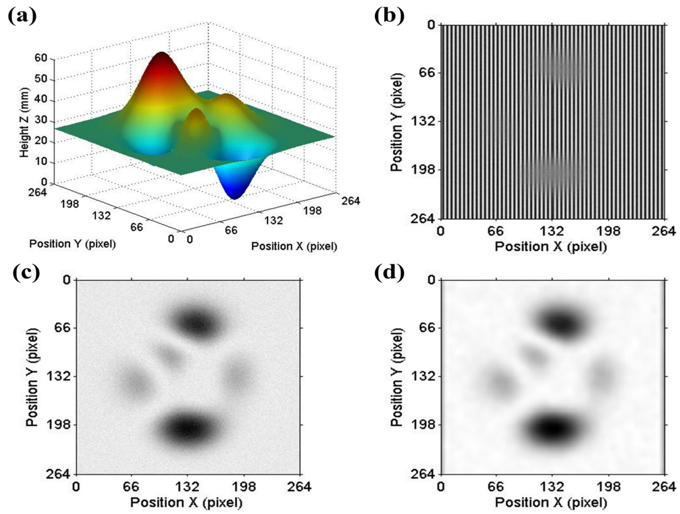

Fig. 4. Simulation: (a) The simulated object; (b) The 60$^{\text{th}}$ frame of fringe pattern; (c) Modulation values obtained by 1DFT; (d) Modulation values obtained by 2DFT.

185–220; columns: 115–150) of the simulated object and the reconstructions of the same area by the two methods. Figure 6(d) shows the part from the 170$^{\text{th}}$ column to the 225$^{\text{th}}$ column in the 100$^{\text{th}}$ row of the simulated object, the same part of the reconstruction by 1DFT and that by 2DFT. For the 1DFT method

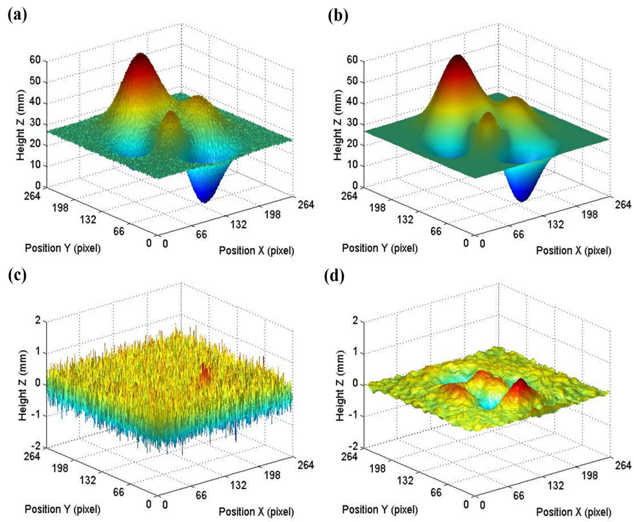

Fig. 5. Simulation results: (a) Reconstruction by 1DFT; (b) Reconstruction by 2DFT; (c) Error distribution by 1DFT; (d) Error distribution by 2DFT.

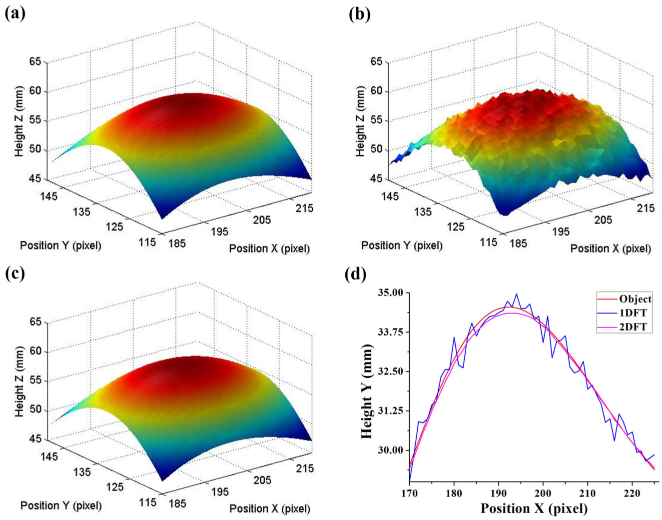

Fig. 6. Comparisons: (a) Part of the simulated object; (b) Part of the reconstruction by 1DFT; (c) Part of the reconstruction by 2DFT; (d) the 170^{th} column to the 225^{th} column in the 100^{th} row of the simulated object, the same part of the reconstruction by 1DFT and that by 2DFT.

in modulation retrieval, calculation result for one pixel in a fringe pattern is extracted from a curve produced by retrieving the same coordinate from the captured fringe patterns, that is, there is no relationship among adjacent pixels, and a slight difference in the modulation values can result in a large difference in height values. This existence of the difference leads to a reconstruction for the measured object with a coarse or irregular surface. However, 2DFT method is a global analysis method. The modulation value of any pixel in the fringe pattern is extracted by taking advantage of the information of pixels in the entire fringe pattern. Besides, the application of the filtering operation brings down steep slopes even though the character of smoothness for the surface shape remains.

4.2 Comparison of Step Surface

To furtherly make a comparison, another computer simulation is used in this section. The simulated object is shown in Fig. 7(a) has a dramatic change in height that there are four discontinuous height steps (10 mm, 30 mm, 50 mm, 70 mm) from the bottom to the top.

In this simulation, the system parameters are the same as those mentioned above. Figure 7 (b) shows the 64^{th} frame of captured images. Figures 7 (c) and (d) are respectively the modulation values of Fig. 7 (b) obtained by 1DFT and 2DFT. Even the measured object has rapid height variation on the shape surface, the application of 1DFT method can obtain accurate modulation value (the edges of the steps are clear) in the areas where height variation is steep. While for the

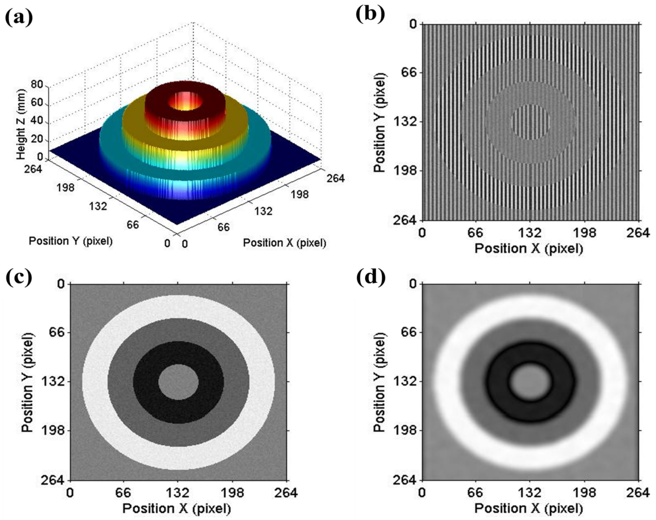

Fig. 7. Simulation: (a) The simulated object; (b) The 60^{th} frame of fringe pattern; (c) Modulation values obtained by 1DFT; (d) Modulation values obtained by 2DFT.

2DFT method, the edge between two steps with different heights is blurred. The reconstructions obtained by the two methods are respectively shown in Figs. 8 (a) and (b). Figures 8 (c) and (d) are the corresponding error distributions. The standard deviation errors are 0.351 mm by 1DFT method and 3.543 mm by 2DFT method. For 2DFT method, due to the filtering operation applied in the analysis of each fringe, high-frequency component containing the details of the measured object is filtered out, the sharp edge of the step becomes smooth. While the result by 1DFT is much better since the modulation is calculated using point-to-point algorithm which eliminates the influence from the neighbor pixels. For clarity, Figs. 9(a)–(c) shows a small area (rows: 195–210; columns: 125–140) on the second step plane of the tested object, the reconstructed result by 1DFT and that by 2DFT. Figure 9(d) shows the part from the 192^{nd} column to the 242^{nd} column in the 152^{nd} row of the simulated object, the same part of the reconstruction by 1DFT and that by 2DFT. For the 1DFT method, the calculation of any point for the height value has no relationship with others that the edge of any two steps can be reconstructed correctly. However, it is the independence of points that the reconstructed plane is not flat (shown in Fig. 9(b)). While for the 2DFT method, the utilization of the filtering operation leads to the result that the high frequency component containing the details of the measured object is filtered out, the sharp edge of the step becomes smooth.

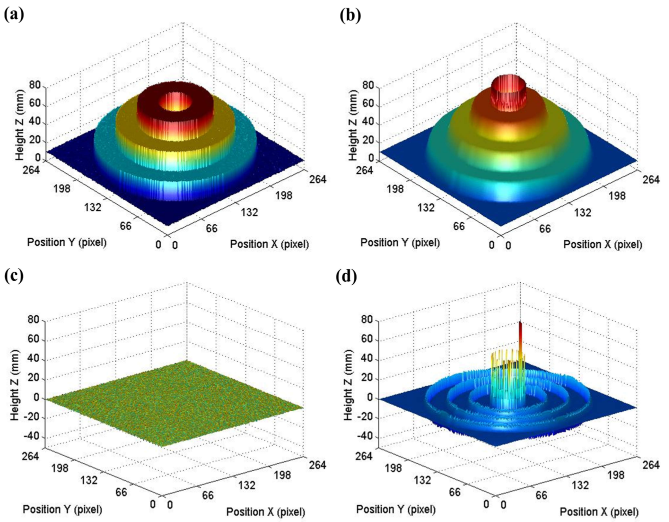

Fig. 8. Simulation results: (a) Reconstruction by 1DFT; (b) Reconstruction by 2DFT; (c) Error distribution by 1DFT; (d) Error distribution by 2DFT.

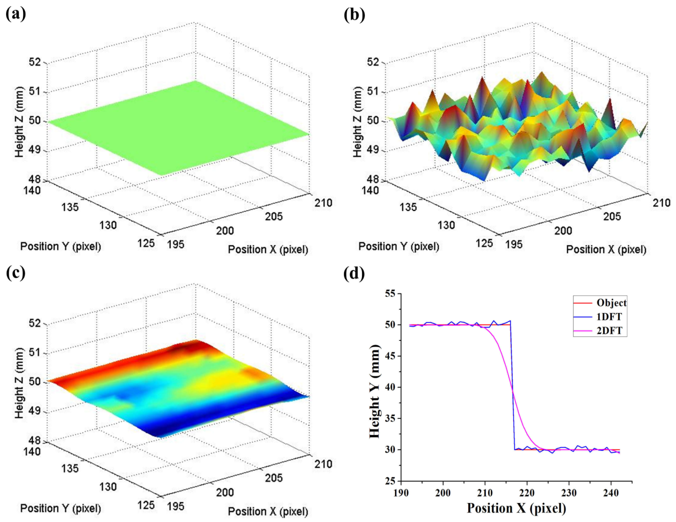

Fig. 9. Comparisons: (a) Part of the simulated object; (b) Part of the reconstruction by 1DFT; (c) Part of the reconstruction by 2DFT; (d) The 192nd column to the 242nd column in the 152nd row of the simulated object, the same part of the reconstruction by 1DFT and that by 2DFT.

5 Experiment

In order to verify the conclusions in the simulation, experiment is carried out to confirm the results. The measurement system is shown in Fig. 10. The grating is 2

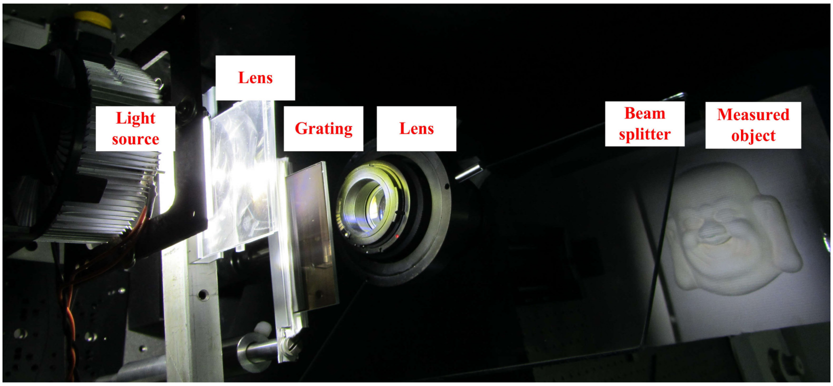

Fig. 10. Configuration of the experiment system.

lines/mm. The face of a Maitreya shown in Fig. 11(a) is utilized as the measured object. In the process of measurement, 471 frames of the fringe patterns are captured by the CCD camera (BASLER A504k). To show the variety of focus plane, Figs. 11(a)–(c) respectively show the 200th, the 300th, the 400th frame of the fringe patterns. It illustrates that the focus plane of the projector changes from top to bottom of the measured object. To reduce the computational work, the size of the captured images is cut to be 880 $\times$ 1030 pixels. Both the 1DFT method and the 2DFT method are applied to analyze the fringes.

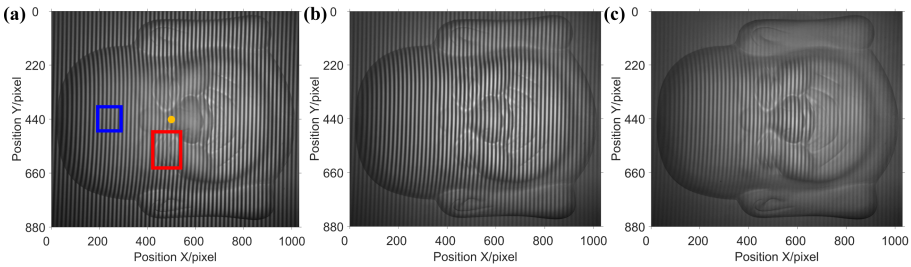

Fig. 11. Fringe patterns: (a) The 200th frame of fringe pattern; (b) The 300th frame of fringe pattern; (c) The 400th frame of fringe pattern. (Color figure online)

For the 1DFT method, the extraction of modulation is done from an angle of an intensity curve formed by eponymous pixels from the captured images. Take the center pixel (441, 515) (marked in Fig. 11(a) with an orange dot) of the cropped image as an example, its intensity cure shows in Fig. 12(a), whose spectrum is shown in Fig. 12(b). Obviously, the spectrum of a cure is very simple, and it's easy for one to filter the useful fundamental frequency information to obtain the envelope of this curve. When the envelope for each pixel is extracted,

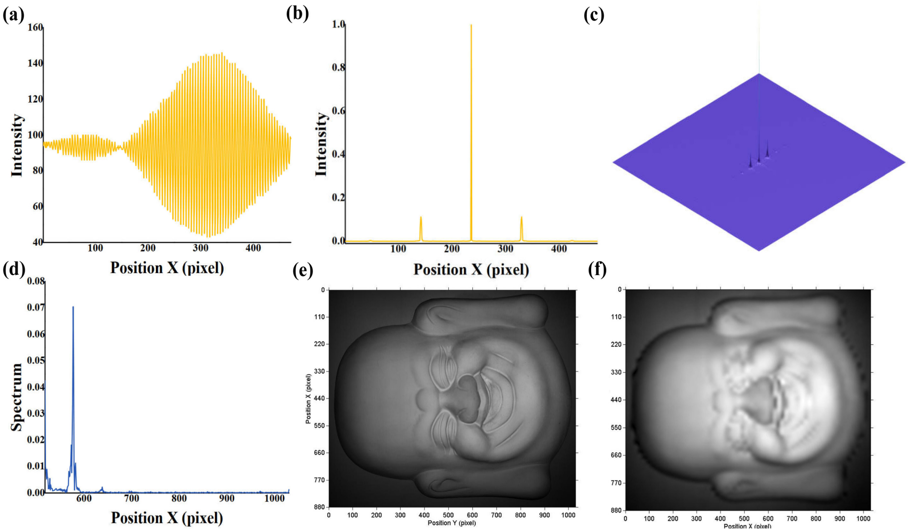

Fig. 12. Modulation retrieval: (a) Intensity curve formed by eponymous pixels from the captured images; (b) The spectrum of (a); (c) The spectrum of Fig. 11(a); (d) Partial cross-section of (c); (e) Modulation values obtained by 1DFT; (f) Modulation values obtained by 2DFT.

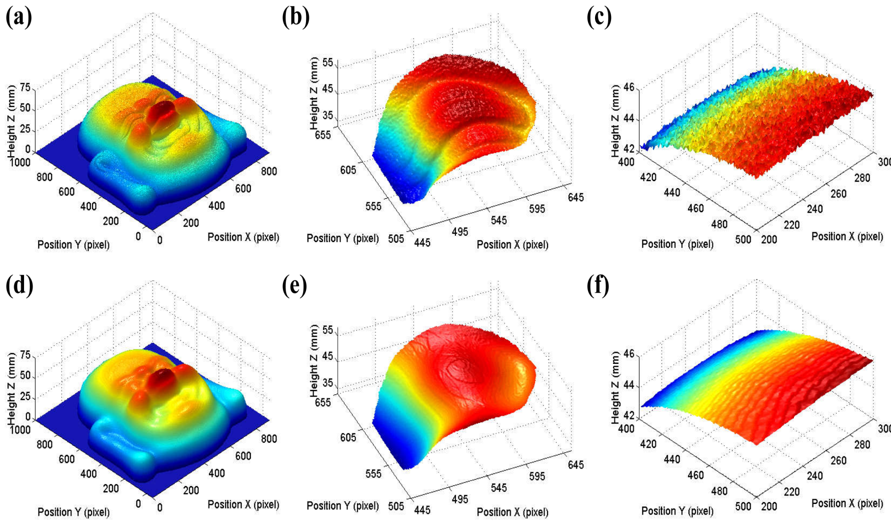

Fig. 13. Experiment results: (a) The reconstruction result obtained by 1DFT; (b) The reconstruction result of the left eye by 1DFT; (c) Enlarged picture of the forehead by 1DFT; (d) The reconstruction result obtained by 2DFT; (e) The reconstruction result of the left eye by 2DFT; (f) Enlarged picture of the forehead by 2DFT.

the modulation distribution for any $t^{\text{th}}(t = 1, 2, 3 \ldots 471)$ fringe can be obtained by extracting the modulation value of the t^{th} point from each envelope line. For the 2DFT method, modulation retrieval is completed from the whole 2D image. Take the 300$^{\text{th}}$ frame of images as an example, its spectrum is shown in Fig. 12(c). It is apparent that the spectrum of a 2D image is more complex than that of a curve. What's worse, the zero-frequency component and high-order frequency component are very close to the fundamental frequency component, and both the zero frequency component and the fundamental frequency component extend to each other. To clearly distinguish the relationship among these frequency components, Fig. 12(d) shows a partial cross-section (row: 441, column: 518–1030) of Fig. 12(c). Figures 12(e) and (f) are the modulation distributions of Fig. 11(b), which are respectively obtained by the 1DFT method and the 2DFT method. Obviously, Fig. 12(e) is clearer than Fig. 12(f). Even for the complex regions such as the nose, the mouth and the eyes, the modulation distribution map can be obtained accurately by 1DFT.

The reconstruction results by the 1DFT method and the 2DFT method are respectively shown in Figs. 12(a)–(c) and Figs. 12(d)–(f). Figures. 12(a) and (d) show the whole surface of the Maitreya by the two methods. For the result obtained by the 1DFT method, the details of the shape surface for the object can be well preserved such as the tiny changes in the eyes, mouth and nose. However, the application of the filtering operation makes the 2DFT method fail to retain the characteristics of these areas with small changes in height. For clarity, Figs. 12(b) and Fig. 12(e) respectively show the height distribution of the left eye (marked in Figs. 11(b) with red rectangle) reconstructed by the two methods. The position of the eyelids can be clearly identified in Fig. 12(b), while Fig. 12(e) just shows a smooth cambered surface that completely misses the details. Figures 12(c) and Fig. 13(f) show the reconstructions of a flat area (part of the forehead marked in Figs. 11(b) with blue rectangle, rows: 401–500; columns: 201–300) calculated by the two methods. Due to the application of point-to-point algorithm for 1DFT, there is no relationship for the calculation of any two adjacent pixels. A slight difference in the modulation values can result in a large difference in height values. Therefore, there are many burrs on the surface shape obtained by 1DFT. While, as shown in Fig. 12(f), 2DFT can reconstruct the corresponding region with a smooth surface.

6 Discussion

In the actual application for the two methods, to get more efficient modulation or improve the measurement accuracy, one can set up the experimental system from the following aspects:

– *Period of the grating.* The period of the grating should be small enough, so that the modulation distribution for each pixel point will be narrow, which helps extract the maximum modulation value and the corresponding serial number more accurately. At the same time, one should take the Nyquist–Shannon sampling theorem into consideration that the sampling period for the fringe pattern should be at last more than 4 points.

- *Pitch and range of grating movement.* The distance of each movement for the grating should be appropriately small to ensure that the modulation curve is sampled properly and smoothly. The entire range of grating movement should be large enough to ensure that the modulation curve includes the maximum modulation value and at least one minimum modulation value adjacent to either side of it.
- *Translation platform.* The grating is driven by a 1D precision translation platform, and this movement is manually controlled. If a closed-loop step-motor control system is utilized, the measurement accuracy will be improved.

7 Conclusion

Two methods including 1DFT method and 2DFT are utilized to extract the modulation distribution of fringe patterns. For 1DFT method, the calculation is completed from an angle of an intensity curve formed by eponymous pixels from a series of captured images, which terminates the influence from the information of other neighbor pixels and can better retain the details of the object under test. While the surface of the reconstruction result will be coarse due to the differences of the modulation values for any adjacent pixels. For 2DFT method, the result is obtained from the perspective of each complete two-dimensional image from the series of the captured fringe patterns, and the application of the filtering operation will smooth the steep edges and corners, bring down a steep slope and fail to retain more details of the measured object.

Acknowledgments. The authors would like to acknowledge the support of the National Natural Science Foundation of China (NSFC) (61801057), Sichuan education department project 18ZB0124, College Students' innovation and entrepreneurship training programs S201910621117 and 202010621108.

References

1. Zhang, S.: Recent progresses on real-time 3D shape measurement using digital fringe projection techniques. Opt. Lasers Eng. **48**(2), 149–158 (2010)
2. Zhang, S.: Absolute phase retrieval methods for digital fringe projection profilometry: a review. Opt. Lasers Eng. **107**, 28–37 (2018)
3. Jiao, D., Liu, Z., Shi, W., Xie, H.: Temperature fringe method with phase-shift for the 3D shape measurement. Opt. Lasers Eng. **112**, 93–102 (2019)
4. Zuo, C., Feng, S., Huang, L., Tao, T., Yin, W., Chen, Q.: Phase shifting algorithms for fringe projection profilometry: a review. Opt. Lasers Eng. **109**, 23–59 (2018)
5. Su, X., Chen, W.: Fourier transform profilometry: a review. Opt. Lasers Eng. **35**(5), 263–284 (2001)
6. Zhang, H., Zhang, Q., Li, Y., Liu, Y.: High speed 3D shape measurement with temporal Fourier transform profilometry. Appl. Sci. **9**(19), 4123 (2019)
7. Zhang, Z., Zhong, J.: Applicability analysis of wavelet-transform profilometry. Opt. Express **21**(16), 18777–18796 (2013)
8. Zhong, J., Weng, J.: Phase retrieval of optical fringe patterns from the ridge of a wavelet transform. Opt. Lett. **30**(19), 2560–2562 (2005)

9. Kocahan, O.: Determination of height profile from a two-dimensional fringe signal using a two-dimensional continuous wavelet transform. Turk. J. Phys. **41**, 81–89 (2017)
10. Stockwell, R.G., Mansinha, L., Lowe, R.P.: Localization of the complex spectrum: the s transform. IEEE Trans. Signal Process. **44**(4), 998–1001 (1996)
11. Zhong, M., Chen, W., Jiang, M.: Application of s-transform profilometry in eliminating nonlinearity in fringe pattern. Appl. Opt. **51**(5), 577–587 (2012)
12. Zhong, M., Chen, W., Wang, T., Su, X.: Application of two-dimensional s-transform in fringe pattern analysis. Opt. Lasers Eng. **51**(10), 1138–1142 (2013)
13. Zhong, M., Chen, W., Su, X., Zheng, Y., Shen, Q.: Optical 3D shape measurement profilometry based on 2D s-transform filtering method. Opt. Commun. **300**, 129–136 (2013)
14. Su, X., Su, L., Li, W.: New Fourier transform profilometry based on modulation measurement. In: Proceedings of SPIE - The International Society for Optical Engineering, vol. 3749 (1999)
15. Su, L., Su, X., Li, W., Xiang, L.: Application of modulation measurement profilometry to objects with surface holes. Appl. Opt. **38**(7), 1153–1158 (1999)
16. Zhong, M., Su, X., Chen, W., You, Z., Lu, M., Jing, H.: Modulation measuring profilometry with auto-synchronous phase shifting and vertical scanning. Opt. Express **22**(26), 31620 (2014)
17. Su, L., Li, W., Su, X., Xiang, L.: Phase-shift error calibration in modulation measurement profilometry. In: 18th Congress of the International Commission for Optics (1999)
18. Mizutani, Y., Kuwano, R., Otani, Y., Umeda, N., Yoshizawa, T.: Three-dimensional shape measurement using focus method by using liquid crystal grating and liquid varifocus lens. In: Proceedings of SPIE - The International Society for Optical Engineering, vol. 6000, pp. 336–431 (2005)
19. Subbarao, M., Gurumoorthy, N.: Depth recovery from blurred edges, pp. 498–503 (1988)